Available online at www.sciencedirect.com
ScienceDirect
Trans. Nonferrous Met. Soc. China 33(2023) 2121−2135
Transactions of Nonferrous Metals Society of China
www.tnmsc.cn

A novel strengthening strategy for diffusion bonded joint of $AlCoCrFeNi_{2.1}$ eutectic high entropy alloy to 304 stainless steel

Peng LI, Hao-tian SUN, Chao LI, Bao-sheng WU, Jiang YANG, Yu JIANG, Hong-gang DONG

School of Materials Science and Engineering, Dalian University of Technology, Dalian 116024, China

Received 2 January 2022; accepted 15 August 2022

Abstract: To explore the potential engineering applications of eutectic high entropy alloys (EHEA), the interfacial microstructure and mechanical properties of the diffusion bonded joint between $AlCoCrFeNi_{2.1}$ EHEA and 304 stainless steel were investigated. The diffusion zone was composed of solid solution zone and Fe_2Al_5 intermetallic compound zone. Due to the difference in the element diffusion rates between the dissimilar base metals and that between the two phases of EHEA, a solid solution region composed of FCC phase and γ-Fe phase is constructed on the EHEA side near the interface, which enhances the shear strength of joint. Besides, the shear strength of joint first increases and then decreases. The maximum shear strength of 355 MPa is obtained at 980 °C, 60 min, and 30 MPa. The interlocking structure and local solid solution structure are formed in the diffusion zone, thus synergistically enhancing the shear strength of joint.

Key words: diffusion bonding; $AlCoCrFeNi_{2.1}$ eutectic high entropy alloy; strengthening mechanism; 304 stainless steel; shear strength

1 Introduction

High entropy alloys (HEAs) are generally composed of at least four principal elements, each with the content of 5−35 at.%, and have attracted extensive attention of scholars in recent years [1,2]. Compared with traditional alloys, HEAs have many excellent properties due to their unique four effects [3−7].

In order to further improve the strength and plasticity of HEAs and increase the castability, LU et al [8,9] designed the $AlCoCrFeNi_{2.1}$ eutectic high entropy alloy (EHEA) with two-phase structure of face centered cubic (FCC) and body centered cubic (BCC), and then obtained the EHEA with both excellent plasticity and high strength. However, the research on HEAs is mainly focused on the composition design, microstructures, mechanical properties, and phase formation, while little on material processing [10,11]. In the actual service process, most parts of nuclear reactor and aeroengine are composed of different materials according to different functions, costs and exposure conditions. Stainless steel (SS) is widely used in manufacture of the core structure, pipeline, heat exchanger and other key parts of nuclear reactor, but its strength, toughness and radiation resistance are weaker than those of HEAs [12]. Therefore, when HEAs are used as structural material in nuclear power plant and other fields, the welding between HEA and stainless steel is required. In fact, in addition to the nuclear industry, composite components welded by dissimilar metals are widely used in modern engineering. Therefore, the weldability of HEAs to traditional metals must be deeply studied to pave the way for their engineering application.

Among all kinds of material processing methods, welding is an ancient yet extensively-used

Corresponding author: Hong-gang DONG, Tel: +86-411-84706283, Fax: +86-411-84709284, E-mail: donghg@dlut.edu.cn
DOI: 10.1016/S1003-6326(23)66248-X

technology in automobile, aerospace and marine industry [13,14], but the research on the welding of EHEAs is still in the initial stage and focused on the homogeneous material [15−18]. In fact, the welding of HEAs to traditional materials is a key technology during actual service process. For example, in the manufacturing of propeller blade, the EHEA/304 stainless steel dissimilar diffusion bonded joints can simultaneously meet the requirements of high strength, good plasticity and low cost. At present, a few scholars have carried out researches on the welding of HEA to stainless steel [19−21]. However, the deformation of fusion-welded joint was large, and the filler metal was required during brazing, which increased the assembly steps and costs.

As a precision welding method, diffusion bonding has the advantages of small deformation and high welding quality, which are especially suitable for the welding of dissimilar materials [22,23]. LI et al [24] found that the shear strength of $AlCoCrFeNi_{2.1}$ EHEA/TiAl alloy dissimilar diffusion bonded joint was increased significantly due to the formation of an interlocking structure in the diffusion zone. DU et al [25] studied the diffusion bonding of $Al_5(TiZrHfNb)_{95}$ refractory high energy alloy to Ti_2AlNb alloy, and found that Al_3Zr_5 could easily cause stress concentration and crack initiation at the phase interface, which has adverse effect on the shear strength of joint. ZHANG et al [26] used Ni interlayer to conduct diffusion bonding of $Co_{28.5}Cr_{21.5}Fe_{20}Ni_{26}Mo_4$ to Inconel 718. When the bonding temperature reached 950 °C, the maximum tensile strength was 1628 MPa under the action of solution strengthening effect at the interface. LI et al [27] investigated the diffusion bonding of $AlCoCrFeNi_{2.1}$ EHEA to GH4169 superalloy, and found that a new layer of FCC solid solution phase was formed in the diffusion zone, which improved the shear strength of joint. It can be seen that dissimilar diffusion bonding joint has a high potential for engineering application. Therefore, diffusion bonding is a suitable method to study the welding of EHEA to stainless steel and can further promote the engineering application of HEAs.

In this work, $AlCoCrFeNi_{2.1}$ EHEA was vacuum diffusion bonded to 304 stainless steel. The microstructure evolution and shear strength of the joints were studied, and the diffusion behavior of alloying elements at different bonding temperatures and bonding time was analyzed in detail. Then, the formation mechanism of solution solid and interlocking structure was clarified.

2 Experimental

The as-cast $AlCoCrFeNi_{2.1}$ EHEA with raw materials of higher than 99.9% in purity and 304 stainless steel were used as base metals. The chemical compositions of base metals are listed in Table 1, and the microstructure of base metals is shown in Fig. 1. It can be seen that the microstructure of EHEA displays eutectic structure composed of B2 phase and FCC phase, while 304 stainless steel contained equiaxed austenite grains.

The base metals were cut into two sizes of 10 mm × 15 mm × 5 mm and 20 mm × 15 mm × 5 mm by wire cutting equipment. Prior to diffusion bonding, the base metals were ground with up to 2000 grit sand paper and then cleaned by ultrasonic equipment. The base metals were assembled as shown in Fig. 1(a) and then put into a diffusion bonding furnace (ZTF2−10, Shanxi Zhituo Solid-State Additive Manufacturing Technology Company, China) under the vacuum degree below 3×10^{-3} Pa. The process curve of diffusion bonding is shown in Fig. 1(b). Generally, the bonding temperature ranges from $0.6T_m$ to $0.8T_m$ (T_m is the lowest melting point of base metals) [28], while the melting points of $AlCoCrFeNi_{2.1}$ EHEA and 304 stainless steel are 1361 and 1440 °C, respectively. Therefore, the temperatures of 880, 930, 980 and 1030 °C were selected for the diffusion bonding process. In order to study the influence of holding time on the quality of joint, the holding time was set as 30, 60 and 120 min, respectively. The holding time of 120 min was set to weaken the influence of sluggish diffusion in EHEA. Besides, the pressure

Table 1 Chemical compositions of $AlCoCrFeNi_{2.1}$ EHEA and 304 stainless steel (wt.%)

Base material	Al	Co	Cr	Fe	Ni	Mn	Mo	Cu	Si	S	P
$AlCoCrFeNi_{2.1}$ EHEA	8.51	18.59	16.40	17.62	38.88	−	−	−	−	−	−
304 stainless steel	−	−	17.15	Bal	8.12	0.78	0.26	0.31	0.65	0.02	0.03

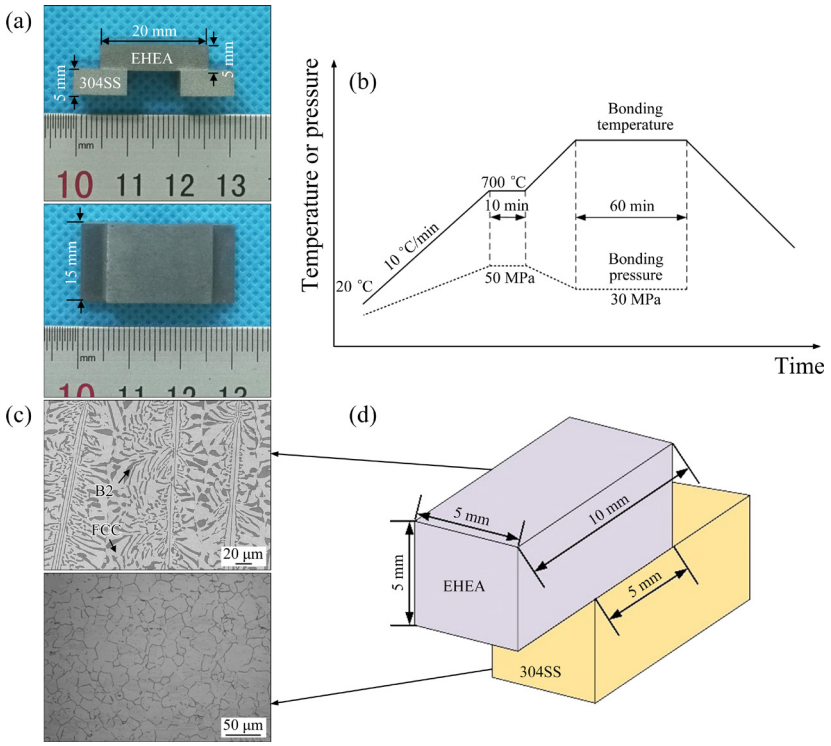

Fig. 1 Appearance of joint (a), process curve of diffusion bonding (b), metallographic structure of base metals (c) and schematic of sample for shear test (d)

of 30 MPa was applied to ensure the close contact of base metals. According to the assembly shown in Fig. 1(a), there are two 75 mm^2 contact areas for the base metals to be welded. Therefore, the required bonding pressure of 30 MPa can be obtained by applying the pressing force on the upper surface of the EHEA.

After diffusion bonding, the joints were cut into the structure shown in Fig. 1(d) by wire cutting equipment, and a fixture was used to grip the sample. The compressive force was applied on the other side of 304 stainless steel at a shear speed of 0.5 mm/min, through which shear force (P) along with the bonding interface was developed and recorded by a universal testing machine (DNS−100, China). During the shear test, the shear stress (τ) can be calculated from the following equation:

$$\tau=P/(ae) \quad (1)$$

where e and a are the height and width of the shear test interface, respectively. After shear test, the fracture surface was observed by scanning electron microscope (SEM, ZEISS−SUPRA55, German) equipped with energy dispersive spectrometer (EDS). The metallographic samples were gradually ground to 2000# and polished with 1.5 μm diamond polishing paste. Then, the evolution of interfacial microstructure and diffusion behavior of samples were investigated by electron probe micro-analyzer (EPMA, JXA−8530 F Plus, Japan).

3 Results and discussion

3.1 Microstructure evolution

Figure 2 shows the evolution of interfacial microstructure from 880 to 1030 °C. The left side is 304SS, while the other side is $AlCoCrFeNi_{2.1}$ EHEA composed of FCC phase and B2 phase. The acicular precipitates composed of B2 phase enriched in Al and Ni elements in FCC phase are coarsened with the increase of temperature, but the distribution is not uniform. The composition of the present B2 phase with ~45 at.% Ni further indicates that one of the lattice sites in B2 unit cell is preferentially occupied by Ni atoms, while other positions are shared by Al and other elements (Co, Cr, and Fe). In the eutectic regions, alternate regions impoverish in Al and rich in Al but impoverish in Fe, Co and Cr are observed. The content of Ni in the B2 phase is much higher than that in the FCC phase. Due to the impoverishment of Ni and Al in FCC phase, the phase stability is maintained by near equiatomic

distributions of Co, Cr, and Fe, which in turn increases the configurational entropy of this phase. The change mechanism of FCC phase in EHEA is mainly terminal migration, and FCC phase with local microstructure coarsening and growth appears at higher temperature. In addition, with the increase of temperature, the lamellar BCC eutectic phase breaks and further refines, and only exists in spherical form. At 930 °C, the microstructure of EHEA is stable, but with the increase of bonding temperature, the thermal stability of microstructure in EHEA gradually decreases, resulting in the gradual decrease of strength and increase of plasticity in EHEA base metal. It is reported that the viscoplastic deformation caused by plastic flow during the diffusion bonding process at elevated temperatures promotes the formation of joint [27]. Therefore, at 980 and 1030 °C, although the strength of EHEA base metal decreases, the strength of joint increases.

The sharp interface exists at all bonding temperatures, and two different regions are formed on both sides of the interface, i.e. Zone I and Zone II. According to the chemical composition of P2 and P5 in Table 2 and the XRD result on joint surface in Fig. 3, Zone I is mainly composed of intermetallic compounds (IMC) enriched with Fe_2Al_5, which is named IMC zone. On the contrary, the chemical composition of P1 in Table 2 shows that Zone II is composed of FCC phase and γ-Fe, which could be named as solid solution zone. Besides, it could be seen from Figs. 2(c, d) that there is a tip diffusion region in the front of the IMC zone, which is caused by the different concentration gradients on both sides of interface. With the increase of bonding temperature, the width

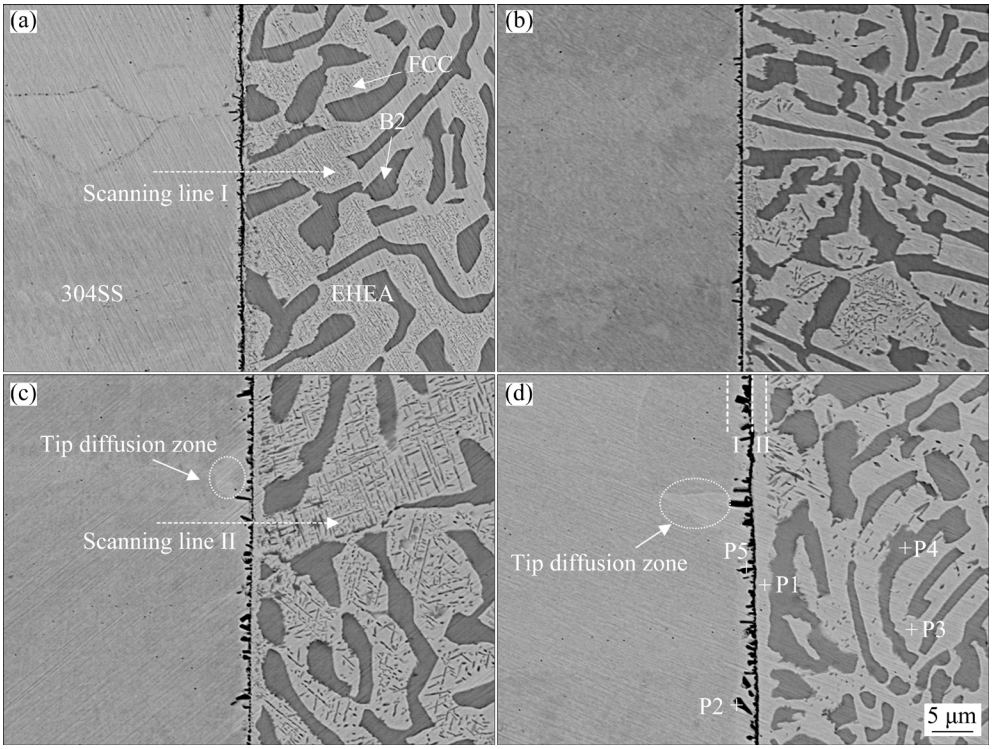

Fig. 2 Microstructures near bonding interface of joints bonded for 60 min under 30 MPa at different temperatures: (a) 880 °C; (b) 930 °C; (c) 980 °C; (d) 1030 °C

Table 2 Chemical composition at locations marked in Fig. 2 (at.%)

Location	Al	Co	Cr	Fe	Ni	Si	Mn	Possible phase
P1	4.89	12.65	18.51	38.29	24.41	0.70	0.55	FCC + γ-Fe
P2	61.91	3.55	6.14	24.16	3.65	0.34	0.25	Fe_2Al_5
P3	9.5	18.6	17.8	18.8	35.3	−	−	FCC
P4	27.5	13.5	8.2	8.6	42.2	−	−	B2
P5	65.84	2.11	4.03	25.18	2.02	0.28	0.54	Fe_2Al_5

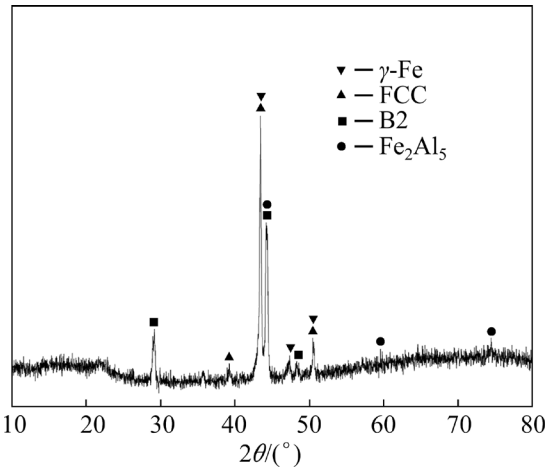

Fig. 3 XRD pattern on fracture surface of joint

of Zone I and Zone II gradually increases. Under the action of higher temperature, the thermal motion of atoms is intenser, and then, the diffusion rate of atoms near the interface increases and the IMCs grow, which leads to the increase of the width of zone near the interface.

Figure 4 shows the microstructure evolution with different holding time. The width of IMC zone and solid solution zone increases with the increase of holding time, while the diffusion rate of elements near the interface increases and the interfacial reaction is intensified, resulting in the growth of IMCs and the widening of solid solution zone. When the holding time reaches 120 min, the width of the diffusion zone increases to 3.23 μm.

3.2 Formation mechanism of IMCs

According to the change of Gibbs free energy, the driving force of phase formation can be calculated as

$$\Delta G=\Delta H-T\Delta S \tag{2}$$

where ΔH and ΔS are the changes in enthalpy and entropy, respectively, T is the thermodynamic temperature. During the solid-state reaction process, LEE et al [29] found that the enthalpy change was much larger than the entropy change, thus ΔG could be approximated to ΔH and the formation enthalpy could be used to predict the formation of phase. PRETORIUS [30] indicated that many factors such as the lowest eutectic point, impurities, and atomic mobility, could affect the actual concentrations that are available for interaction at the growth interface. Therefore, the concept of effective concentration

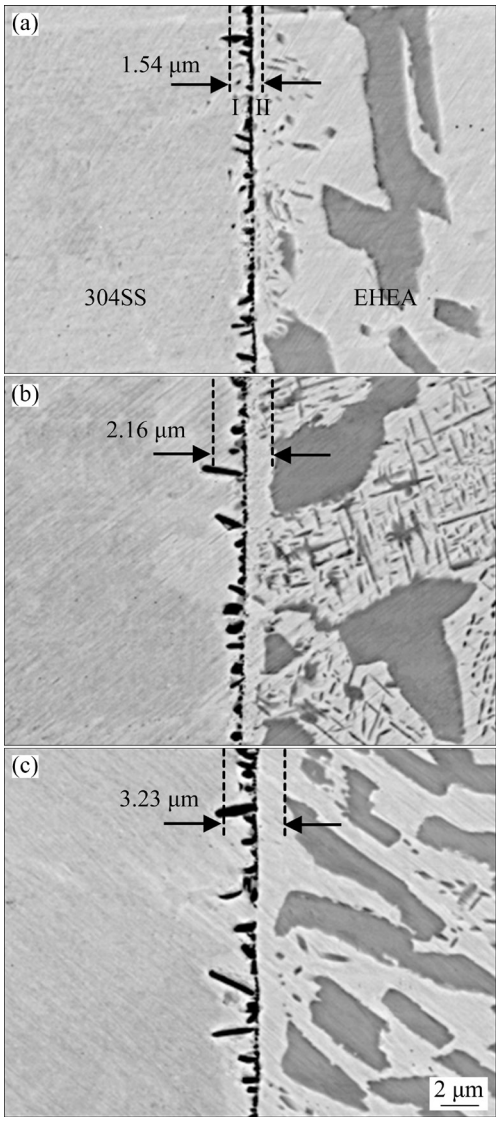

Fig. 4 Microstructures of joints bonded at 980 °C under pressure of 30 MPa for different time: (a) 30 min; (b) 60 min; (c) 120 min

was proposed in the calculation of effective enthalpy of formation as follows [31]:

$$\Delta H'=\Delta H\cdot E/C \tag{3}$$

where E is the effective concentration limiting element, and C is the compound concentration limiting element. Figure 5 shows the effective enthalpy of formation of different Al−Fe phases, and it can be seen that $\Delta H'_{Fe_3Al} > \Delta H'_{FeAl_2} > \Delta H'_{FeAl_3} > \Delta H'_{Fe_2Al_5}$. Because Fe_2Al_5 has the lowest effective enthalpy of formation, Fe_2Al_5 is the first product and then is preferentially formed at the interface, which is consistent with this experimental result. However, due to the sluggish diffusion effect of HEAs, the diffusion rate of Al in EHEA is much

lower than that in aluminum alloy, resulting in the weak binding ability of Al and Fe, and then no other products such as $FeAl_3$ and $FeAl_2$ appear at the interface.

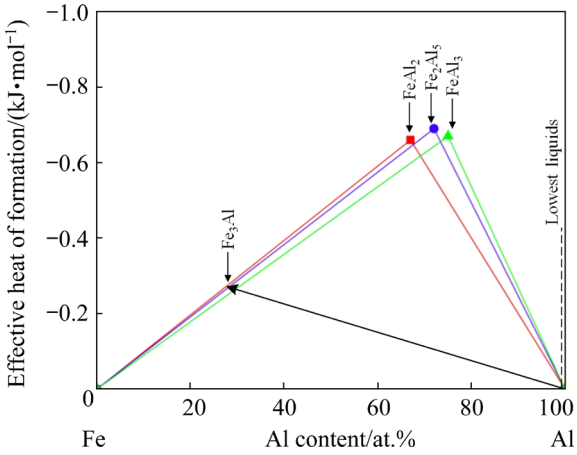

Fig. 5 Effective enthalpy of Fe−Al formation diagram

The sluggish diffusion effect of HEAs refers to the sluggish phenomenon of atomic diffusion and phase transition kinetics caused by the special lattice structure in HEAs. The sluggish diffusion effect can be analyzed from an energy point of view. Due to the different atomic configurations near each lattice in HEAs, the migration of atoms in different positions require different activation energies. When an atom jumps into a vacancy in a lower-energy state, it needs a higher activation energy to jump out of this position, which is not conducive to its continued migration. Conversely, when an atom jumps into a vacancy in a high-energy state, it tends to jump back to its original node. Clearly, both cases slow down the diffusion process of atoms. In traditional alloys, due to the low concentration of solute, the atomic configurations around the junction before and after atomic migration are very similar, which is conducive to atomic diffusion. The sluggish diffusion effect not only affects the phase transformation process of HEAs, but also affects the crystal structure and performance. This is because the slow diffusion rate can effectively delay the nucleation and growth of HEAs, thereby promoting the formation of nanocrystals and amorphous structure. The formation of amorphous structure increases the hardness and soft magnetic properties of HEAs. In addition, the sluggish diffusion effect can also improve the high-temperature performance of HEAs, such as high-temperature strength, high-temperature structural stability and creep resistance.

Figure 6 shows the schematic growth of Fe_2Al_5. At the initial stage, it can be seen that a large number of Fe_2Al_5 nucleates at the interface, and there is no obvious orientation of nuclei at the interface. At the end of nucleation, Fe_2Al_5 is formed and initially grows at the initial interface, and then the grains of Fe_2Al_5 further grow under the diffusion reaction of Fe and Al. During the process of solid phase diffusion, the Al atoms mainly diffuse towards the stainless steel side through the Fe_2Al_5 zone, and only when Al diffuses to the front of Fe_2Al_5 can it react with Fe to form Fe_2Al_5, which leads to the growth of Fe_2Al_5 towards the stainless

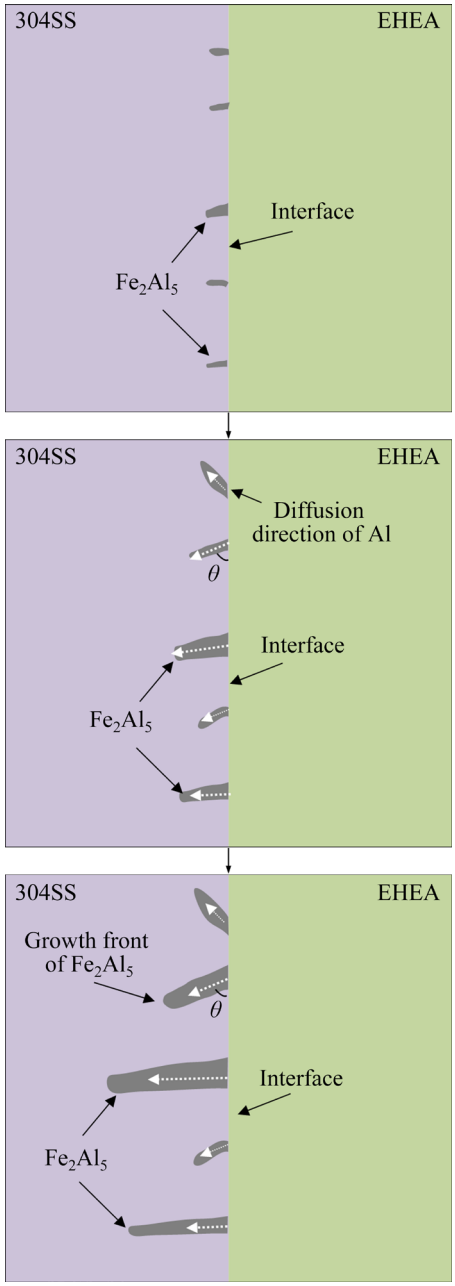

Fig. 6 Schematic growth of Fe_2Al_5

steel side. Besides, the growth rate towards the stainless steel side of grains in some directions is much faster than that of other nuclei at the interface, which shows a dominant growth. The reason for this phenomenon is that the orientation angle θ of these grains approaches 90°, and the diffusion direction of Al atom is consistent with its growth direction, resulting in the growth rate much higher than that of other grains. This phenomenon indicates that there is an obvious competitive growth mechanism at the interface, and then the growth of the grains with other orientations are seriously inhibited in the subsequent process. The growth of Fe_2Al_5 at the interface leads to the formation of serrated interlocking structure, which is expected to improve the mechanical properties of joint. The interlock structure formed by metallurgical reaction is more precise and controllable than that formed by mechanical force, and the diffusion of elements is difficult to produce microcracks and other defects, so that the joint has better mechanical properties and interface controllability.

3.3 Elemental distribution and diffusion behavior

The line scanning analysis results from stainless steel side to FCC phase side and to B2 phase side are shown in Figs. 7(a, b), respectively. Due to the precipitation of a small amount of B2 phase in FCC phase in EHEA, the fluctuation of elements appears on EHEA side, which shows that the contents of Al and Ni increase, while the contents of Fe, Co and Cr decrease. The Al element diffuses from EHEA side to the stainless steel side, and content of Al increases sharply in IMC zone. Because the content of Al is much higher than that in stainless steel, a large concentration gradient is formed near the interface, which leads to the rapid diffusion of Al to the stainless steel side. Then, a large amount of Fe elements on the stainless steel side react with Al element. According to the analysis in Section 3.2, Fe_2Al_5 has the lowest effective enthalpy of formation, which leads to the formation of Fe_2Al_5 prior to other IMCs at the interface near stainless steel side.

It can be seen from Fig. 7(b) that compared with the black B2 phase in EHEA, the contents of Al and Ni in Zone II decrease, while the contents of Fe, Co and Cr increase significantly, further indicating that this zone is a solid solution composed of FCC and γ-Fe. The formation of this zone is caused by the following two aspects. One is that the diffusion rate of Fe in stainless steel is much higher than that of Fe, Cr and Co in EHEA. Due to the sluggish diffusion effect, the elements in EHEA are restrained from diffusing into the stainless steel side, and then the Fe element tends

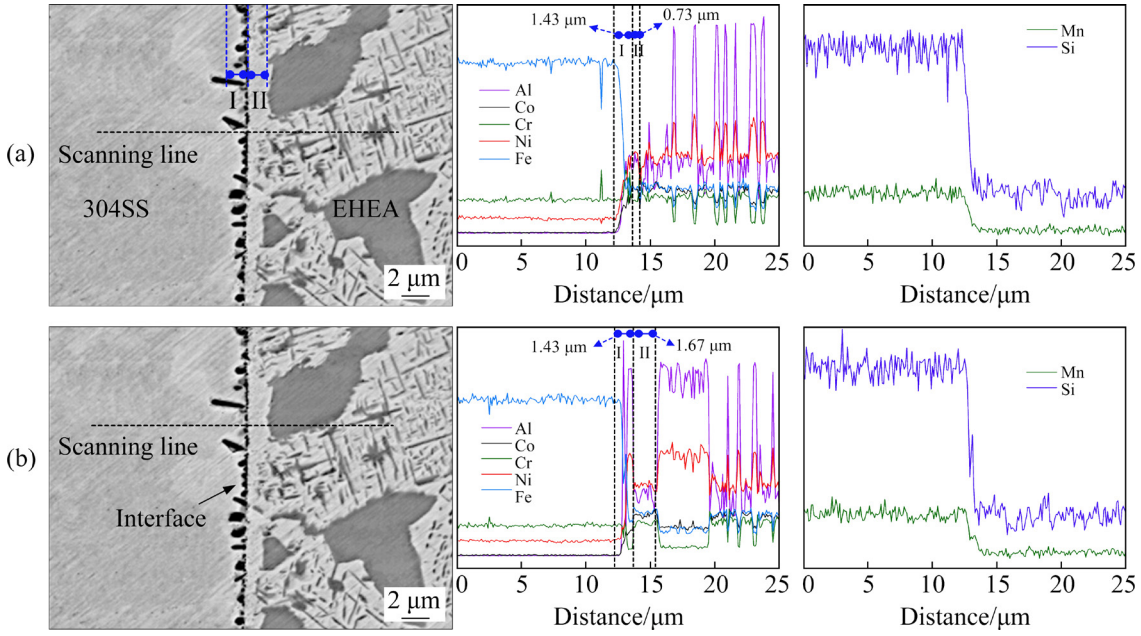

Fig. 7 Results of line scanning analysis on joints bonded at 980 °C under 30 MPa for 60 min near FCC phase (a) and B2 phase (b)

to diffuse to the EHEA side in a relatively unidirectional way, resulting in the formation of γ-Fe on the EHEA side of the interface.

Besides, compared with the elements of Al and Ni in B2 phase, the element of Fe in stainless steel has better affinity with Fe, Cr and Co in FCC phase, which leads to the formation of FCC phase in this zone. LIU et al [28] studied the diffusion bonding of CoCrFeMnNi HEA to T2 copper, and found that the diffusion rate of Cu on EHEA side was much higher than that of EHEA on Cu side. This result showed that the solid solution metallurgical structure could be formed near the interface, which was similar to this study. Another aspect is that the diffusion rate of atoms in FCC phase is different from that in B2 phase. The diffusion rate of atoms near the interface is affected not only by the concentration gradient, but also by the sluggish diffusion effect of EHEA. When the concentration gradient of elements near the interface is large, the diffusion rate of atoms is controlled by the concentration gradient, such as the atom of Al. But with the decrease of concentration gradient, the diffusion rate of atoms is dramatically affected by sluggish diffusion effect, such as the atoms of Co, Fe and Cr. For Al−Co−Cr−Fe−Ni system, the sequence of diffusion rate is similar as previously-reported HEAs: Ni < Co < Fe < Cr [32]. Because Ni has the lowest diffusion rate, the FCC phase rich in the elements of Fe, Co and Cr is formed near the interface. Besides, the width of Zone II in Fig. 7(b) is wider than that in Fig. 7(a), indicating that the width of solid solution zone in front of B2 phase is wider than that in front of FCC phase. The reason for this phenomenon is that the elements of Co, Fe and Cr are hindered by the B2 phase dispersed in the front of FCC phase during the diffusion bonding process, which leads to the accumulation of elements in the front of B2 phase matrix and the increase of the width in diffusion zone. Among the trace elements, the elements of Mn and Si diffuse from the stainless steel side to the EHEA side under the effect of high concentration gradient.

Figure 8 shows the results of line scanning analysis at different temperatures. With the increase of bonding temperature, the distance of diffusion zone near interface increases from 1.65 to 2.16 μm. Relationship between temperature and diffusion coefficient obeys the Arrehenius formula [33]:

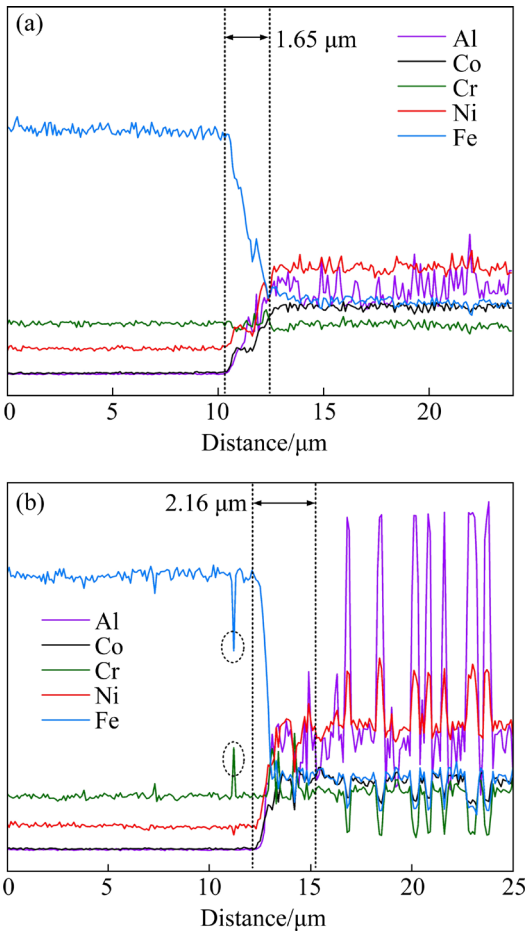

Fig. 8 Results of line scanning analysis on joints bonded at different temperatures: (a) 880 °C; (b) 980 °C

$$D=D_0\exp[-Q/(RT)] \quad (4)$$

where Q is the activation energy of diffusion, D_0 is the diffusion constant (m^2/s), and R is the molar gas constant (8.314 J/(mol·K)). It can be seen that the diffusion coefficient increases with the increase of temperature, which leads to sufficient diffusion of the elements and wider diffusion zone. Besides, the increase of temperature and holding time promotes the viscoplastic deformation of joint, and then the number of voids at the interface decreases, further leading to the sufficient diffusion of elements and severe interface reaction.

The elemental mapping distribution near the interface of joint bonded at 980 °C is shown in Fig. 9. The B2 phase in EHEA is enriched in the elements of Al and Ni, while the FCC phase is enriched in the elements of Fe, Co and Cr. It can be also seen that the Al element is enriched in Zone I, and the content of Fe is lower than that of stainless steel, which further indicates that the composition

in Zone I is Fe_2Al_5 IMC. However, the elements of Fe, Co and Cr are enriched in Zone II, which indicates that the zone is composed of FCC phase and γ-Fe. It is worth noting that the elements of Fe, Ni and Co appear in the front of Fe_2Al_5, thus forming a tip diffusion zone. After the formation of IMC zone, a diffusion channel is formed between the Fe_2Al_5 and stainless steel, then a few atoms of Fe, Ni and Co enter the stainless steel along the diffusion channel with a low concentration gradient, and finally gather in the front of Fe_2Al_5. However, due to the higher content of Cr in stainless steel, the concentration difference between the two sides of the interface is small, and no obvious diffusion of elements appears.

3.4 Growth behavior of different layers in diffusion zone

The average interfacial thickness of the joints is shown in Fig. 10. The diffusion rate of atoms increases under the action of high temperature, and at the same time, the width of IMC zone and solid solution zone gradually increases under the long-time action. It can be seen from Fig. 10(a) that the width of solid solution zone in front of FCC phase increases significantly at 1030 °C. According to previous studies, 1000 °C was the critical temperature for the diffusion of HEAs [22]. When the temperature is lower than 1000 °C, the diffusion of elements is affected by the sluggish diffusion effect of EHEA. In HEAs, different atoms occupy the lattice randomly, and each atom is surround by others, which requires the coordination of different kinds of elements during the diffusion process. Therefore, the diffusion resistance increases and the diffusion rate of element decreases, resulting in the narrowing of IMC zone and solid solution zone. However, when the temperature is over 1000 °C, the atoms are easy to jump into the vacancy, and then the diffusion rate of element increases, which leads to sufficient diffusion of the element and weakens the influence of sluggish diffusion effect.

To further reveal the effect of bonding temperature on the diffusion behavior of IMC zone and solid solution zone, the fitted growth curve and growth activation energy are investigated. For diffusion bonding, the relationship between thickness of IMC zone and solid solution zone and

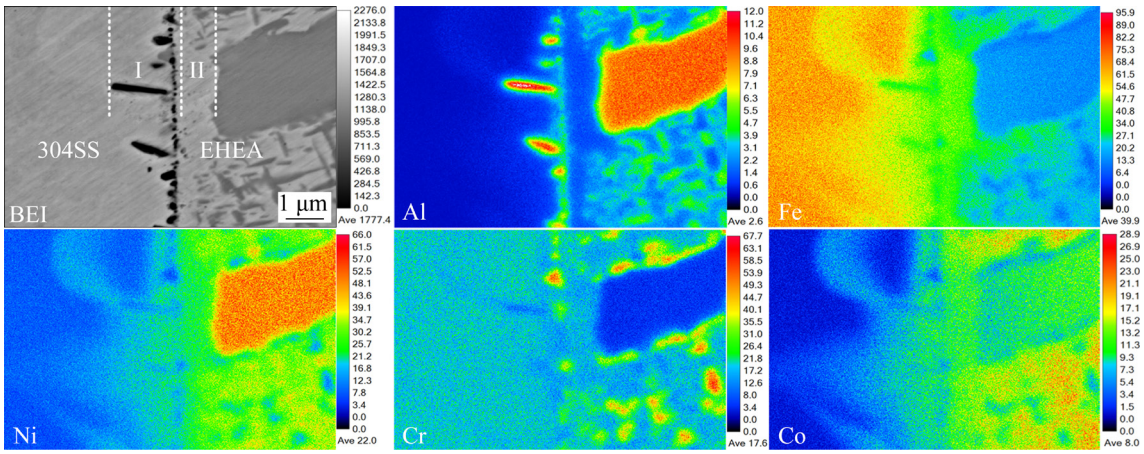

Fig. 9 Elemental mapping distributions of joint bonded at 980 °C

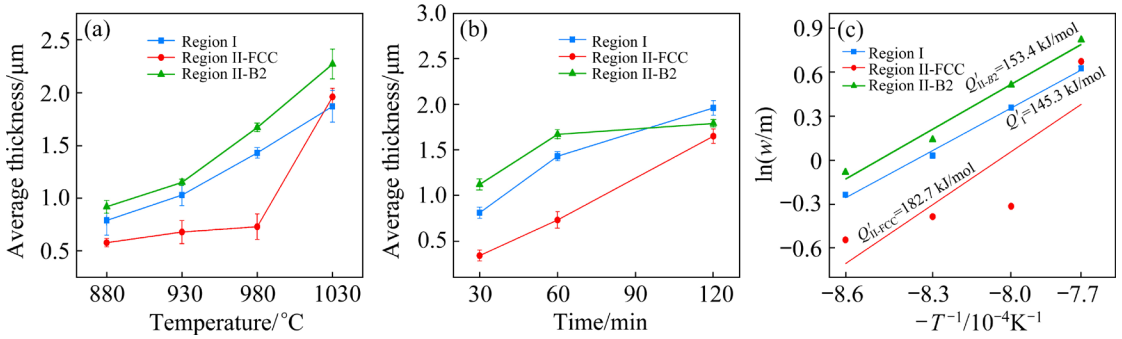

Fig. 10 Average interfacial thickness of joints bonded with different parameters: (a) 880−1030 °C, 60 min, 30 MPa; (b) 980 °C, 30−120 min, 30 MPa; (c) Growth activation energy of different layers

reaction time can be described as [34]

$$w^2=kt \quad (5)$$

$$k=k_0\exp[-Q'/(RT)] \quad (6)$$

where k is the growth rate, k_0 is the pre-exponential factor, w is the thickness of diffusion layers, t is the reaction time, and Q' is the growth activation energy. In this work, the reaction time is constant of 60 min and the bonding temperature is variable. By combining Eqs. (5) with (6), a new equation about the relationship between thickness of IMC zone and solid solution zone and temperature can be deduced as follows:

$$\ln w=1/2\ln(k_0t)-Q'/(2RT) \quad (7)$$

Figure 10(c) shows the fitting results about the growth activation energy of different layers. Region I has the lowest growth activation energy of 145.3 kJ/mol, indicating that the region first grows when the bonding temperature is increased. In Region II, the growth activation energy of the front region of B2 phase is 153.4 kJ/mol, which is lower than that of the front region of FCC phase, indicating that the solid solution region is first formed in the front region of B2 phase. Based on the above results, it can be seen that during the diffusion bonding process, Fe_2Al_5 IMCs are first formed near the interface, and then the solid solution zone composed of FCC phase and γ-Fe is formed in the front region of B2 phase under the diffusion action of Fe, Co and Cr. Finally, with the increase of temperature, the diffusion rate of elements increases and then the solid solution zone is formed in the front region of FCC phase.

3.5 Mechanical properties

The shear strength of joints bonded at different temperatures is shown in Fig. 11(a). The shear strength of joint is 217 and 264 MPa at 880 and 930 °C, respectively. With the bonding temperature increasing to 980 °C, the shear strength of the joint reaches 355 MPa, while the joint strength decreases to 347 MPa when the temperature is increased to 1030 °C. There are two reasons for the highest shear strength of the joint bonded at 980 °C. First, the interlocking structure composed of Fe_2Al_5 IMC improves the shear strength of joint. When the temperature is lower than 980 °C, due to insufficient

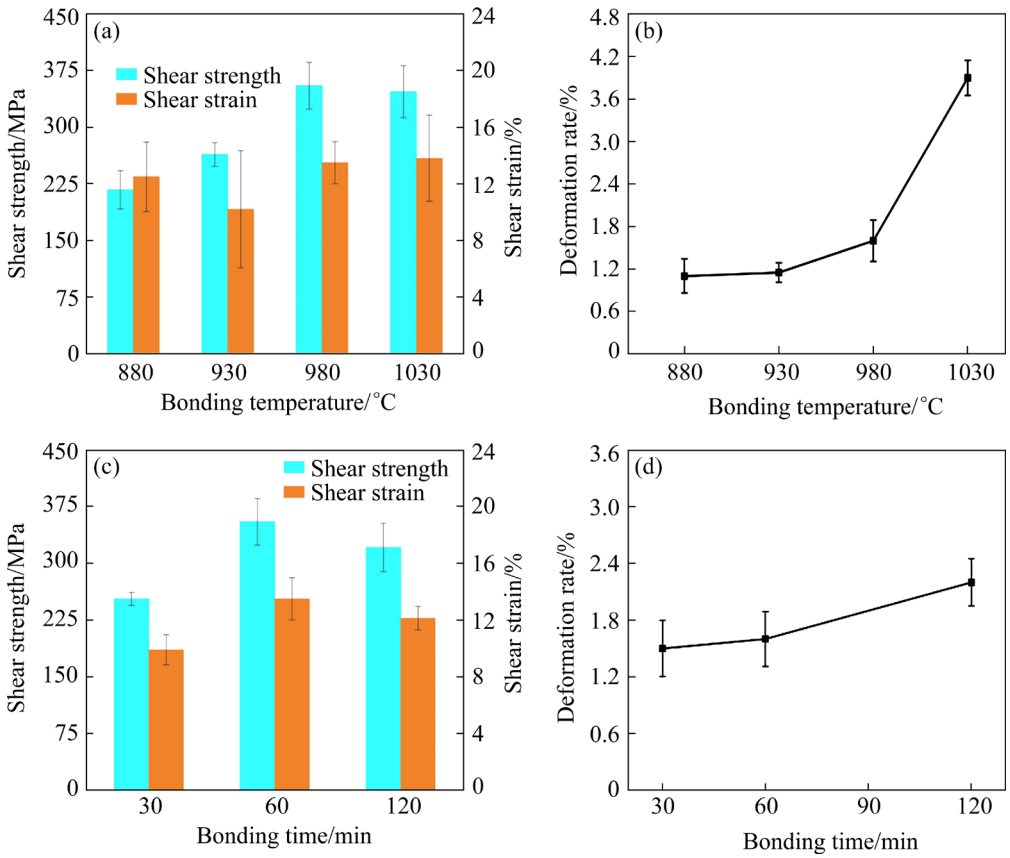

Fig. 11 Mechanical properties of joints bonded at different temperatures for 60 min (a, b) and bonded at 980 °C for different time (c, d): (a, c) Shear strength and shear strain; (b, d) Deformation rate

diffusion of Al element, Fe_2Al_5 cannot grow up, resulting in weak interlocking effect and low shear strength.

In addition, due to the existence of the critical thickness of IMCs, the mechanical properties of joint will deteriorate when the thickness exceeds the critical value [35]. Therefore, at 1030 °C, the overgrowth of Fe_2Al_5 results in the increase of the thickness of reaction layer and the decrease of shear strength. The second reason is the width of solid solution zone. The formation of solid solution zone on the side of EHEA indicates local solid solution near interface, which can improve the mechanical properties of joint from the metallurgical aspect. With the increase of temperature, the solid solution zone is widened gradually, and then the solution strengthening effect is enhanced, which increases the shear strength. In conclusion, under the synergistic effect of interface interlocking structure and local solid solution, the maximum shear strength of joint reaches 355 MPa, which is equivalent to the strength of base metal. Besides, the shear strain is larger than 10% at all temperatures. When the bonding temperature reaches 980 °C, the shear strain is 13.5%, which indicates that the joint has an excellent plasticity at this temperature.

The deformation rate of joints bonded at different bonding temperatures is shown in Fig. 11(b). With the increase of the bonding temperature, the deformation rate increases gradually. In the temperature range from 880 to 980 °C, the deformation rate of joint is less than 2%. When the bonding temperature is higher than 1000 °C, the interfacial formation mechanism of high entropy alloy diffusion bonded joint is changed from diffusion to viscoplastic deformation. When the bonding temperature reaches 1030 °C, the deformation rate increases sharply to 3.9%, which is related to the change of interface disappearance mechanism from diffusion to viscoplastic deformation. Although the viscoplastic deformation mechanism can promote the disappearance of interface, the deformation rate of joint increases. Therefore, in practical engineering application, considering the shear strength and deformation rate of joint, the bonding temperature of 980 °C is suggested for diffusion bonding process.

Figure 11(c) shows the shear strength with different holding time. With the prolongation of holding time, the shear strength of joint first increases and then decreases. When the holding time is 60 min, the shear strength of joint reaches 355 MPa. With the increase of holding time from 30 to 60 min, sufficient diffusion occurs near the interface, and the Fe_2Al_5 IMCs grow, which leads to the increase of interlocking structure and local solid solution structure near the interface and the enhancement of joint strength. However, when the holding time is continuously prolonged to 120 min, Fe_2Al_5 IMCs near the interface grow violently and exceed the critical thickness, resulting in the decrease of joint strength. As shown in Fig. 11(d), the deformation rate of joint increases with the prolongation of holding time, but the deformation rate is less than 2.5% at all holding time, indicating that no severe deformation appears in the joint. According to Fig. 11, the optimum process parameters for diffusion bonding of EHEA to stainless steel are 980 °C, 60 min and 30 MPa, and the shear strength and deformation rate of joint are 355 MPa and 1.6%, respectively, which indicates that the joint has high strength and low deformation rate with these process parameters.

The tensile strength and elongation of EHEA are 911.8 MPa and 11.7%, and the tensile strength of 304SS is 520 MPa. Although the shear strength lacks relevant data, from Refs. [19−21,36], the shear strength of metal is about 60% of the tensile strength [37], and thus it is speculated that the tensile strength in this study is about 592 MPa, which is higher than the strength of 304SS base metal. Figure 12 shows the comparison of joint

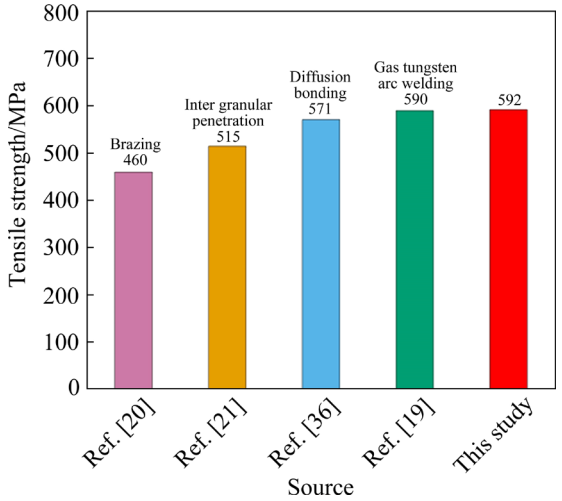

Fig. 12 Comparison of tensile strength of joint between this study and other studies [19−21, 36]

strength between this study and others. It can be seen that the tensile strength of the joint obtained in this study is equivalent to that obtained by gas tungsten arc welding. However, due to the large deformation of the joint obtained by fusion welding, the diffusion bonding method is more suitable for the bonding between EHEA and stainless steel. Besides, due to the synergistic effect of local solid solution structure and interlocking structure, the joint strength of diffusion bonding obtained in this study is higher than that of the previously-reported counterpart.

3.6 Fracture morphology

Figure 13(a) shows the fracture path of the joint bonded at 980 °C after shear test. The serrated structure appears near the interface at stainless steel side, which indicates that the fracture occurs in the interlocking structure composed of Fe_2Al_5 IMCs. Compared with the solid solution zone, IMC zone has larger brittleness and becomes the weak zone of joint. However, due to the formation of serrated interlocking structure, the shear strength increases in IMC zone, resulting in the enhancement of shear strength of the whole joint.

As shown in Fig. 13, the fracture surfaces of joint bonded at 930 °C are flat with shear bands, indicating a brittle fracture feature. When the bonding temperature raises to 1030 °C, the river pattern formed by cleavage step expansion appears on the fracture surface of the EHEA side, while the dimples of microporous aggregation appears on the stainless steel side, indicating the occurrence of quasi-cleavage fracture. A large area of smooth zone exists on the fracture surface, which is formed by the fracture of FCC phase with good plasticity. And a small amount of cleavage steps exists in the smooth zone, which are formed by the fracture of hard and brittle B2 phase. Because FCC phase has more slip systems, continuous plastic deformation can occur through dislocation slip and then the plastic fracture occurs, while BCC phase has less slip systems and brittle fracture can only occur along a specific crystal plane. Besides, during the plastic deformation process, the FCC phase with good plasticity hinders the formation of cracks and enhances the plasticity of joint. Table 3 shows that a solid solution zone composed of FCC phase and γ-Fe appears on the EHEA side, and then increases the shear strength of joint. However, the peeling of solid solution occurs at P6. Because the solid solution zone in the front of FCC phase has the

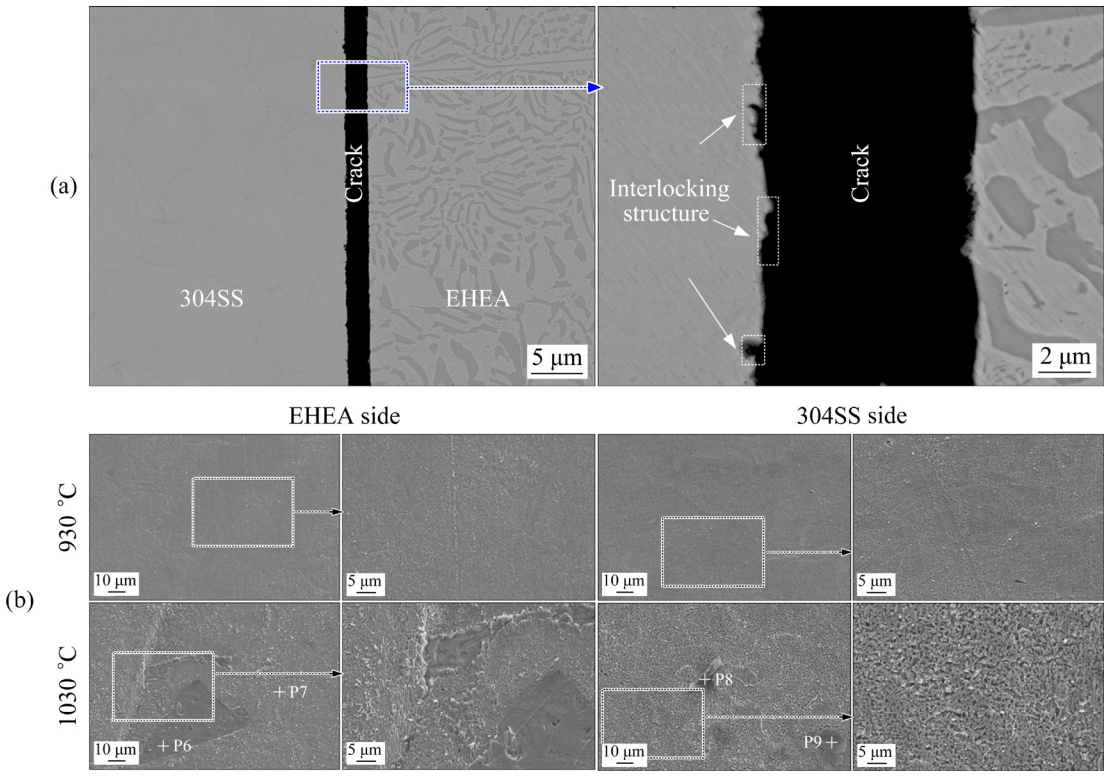

Fig. 13 Fracture path of joints bonded at 980 °C (a) and fracture morphologies on resultant joints bonded at different temperatures for 60 min (b)

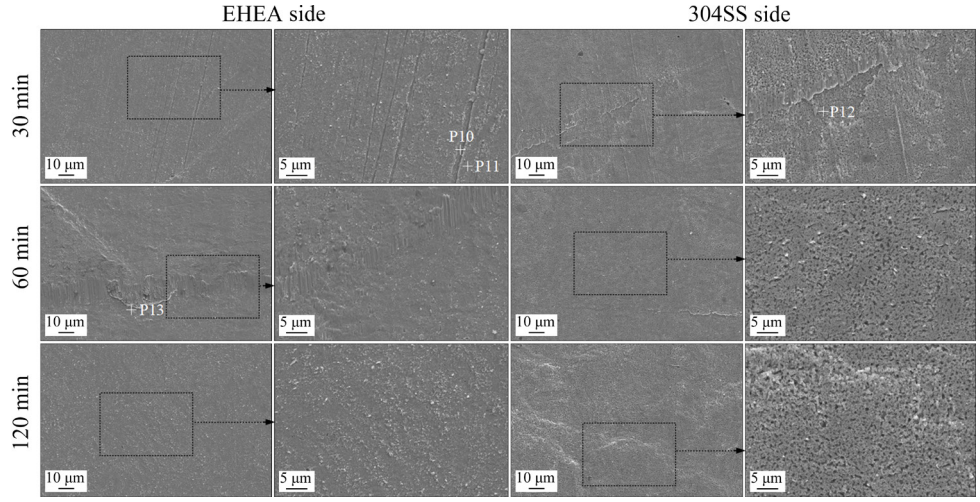

Fig. 14 Fracture morphologies of resultant joints bonded at 980 °C for different time

Table 3 Chemical compositions at locations marked in Figs. 13 and 14 (at.%)

Location	Al	Co	Cr	Fe	Ni	Si	Mn	Possible phase
P6	5.11	23.14	21.48	24.24	26.03	–	–	FCC
P7	4.38	12.54	24.88	37.57	19.55	0.65	0.43	FCC + γ-Fe
P8	58.1	3.19	4.41	25.42	8.06	0.59	0.23	Fe_2Al_5
P9	63.43	2.01	4.36	24.18	5.08	0.78	0.16	Fe_2Al_5
P10	5.51	20.61	21.53	24.72	27.63	–	–	FCC
P11	4.55	11.62	17.24	40.74	25.3	0.34	0.21	FCC + γ-Fe
P12	2.32	2.78	18.56	69.32	6.32	0.46	0.24	γ-Fe
P13	3.05	7.73	18.36	52.11	18.28	0.28	0.19	FCC + γ-Fe

highest activation energy, the width is the narrowest and the generation speed is the slowest in this zone, which leads to the peeling during shear test. According to the chemical composition of P8 and P9, there are still residual Fe_2Al_5 IMCs on the fracture surface of stainless steel, which further proves that the interlocking structure composed of Fe_2Al_5 IMCs can improve the shear strength of joint.

Figure 14 shows the fracture morphology of the joints bonded for different holding time. When the holding time is 30 min, the fracture surface is flat, and the peeling of solid solution occurs at many positions. However, with the prolongation of holding time, the dimples of microporous aggregation appear on the fracture surface of stainless steel side, and no obvious peeling phenomenon of solid solution zone occurs on the EHEA side. With the prolongation of holding time, the effect of solid solution strengthening increases gradually, and then the joint strength is enhanced.

4 Conclusions

(1) Sound joint of $AlCoCrFeNi_{2.1}$ EHEA and 304 stainless steel is obtained by diffusion bonding. With the temperature increasing and the holding time prolonging, the shear strength of joints gradually increases, and the maximum value of 355 MPa is obtained at 980 °C, 60 min and 30 MPa. The fracture of joint occurs in the Fe_2Al_5 intermetallic compound zone on the stainless steel side.

(2) The diffusion zone is composed of solid solution zone and Fe_2Al_5 intermetallic compound zone. With the increase of bonding temperature and holding time, the diffusion zone is gradually widened. The interlocking structure and local solid solution structure are formed in the diffusion zone, which synergistically enhances the shear strength of joint.

(3) A solid solution zone composed of FCC phase and γ-Fe phase is formed on the high entropy

alloy side due to the difference of physical properties between the stainless steel and high entropy alloy, as well as different element diffusion rates of FCC phase and B2 phase in high entropy alloy. The width of solid solution zone in front of B2 phase is larger than that in front of FCC phase.

Acknowledgments

This work was financially supported by the National Natural Science Foundation of China (No. 52075074), the Science and Technology Plan of Liaoning Province, China (No. 2021-MS-117), the Fundamental Research Funds for the Central Universities, China (DUT21JC16), and technically supported by the Collaborative Innovation Center of Major Machine Manufacturing in Liaoning Province, China.

References

[1] YEH J W, CHEN S K, LIN S J, GAN J Y, CHIN T S, SHUN T T, TSAU C H, CHANG S Y. Nanostructured high-entropy alloys with multiple principal elements: Novel alloy design concepts and outcomes [J]. Advanced Engineering Materials, 2004, 6: 299−303.

[2] CANTOR B, CHANG I T H, KNIGHT P, VINCENT A J B. Microstructural development in equiatomic multicomponent alloys [J]. Materials Science and Engineering A, 2004, 375: 213−218.

[3] DU Hui, CAI Jia-hong, WANG Ya-song, YAO Jun-qing, CHEN Qiang, CUI Yu, LIU Xin-wang. Effect of partial recrystallization on microstructure and tensile properties of NiFeCoCrMn high-entropy alloy [J]. Transactions of Nonferrous Metals Society of China, 2022, 32: 947−956.

[4] ZHANG Lin, SONG Ruo-kang, QU Guo-xin, LU Tong. Effect of nitrogen on microstructure and mechanical properties of $CrMnFeVTi_6$ high entropy alloy. [J]. Transactions of Nonferrous Metals Society of China, 2021, 31: 2415−2427.

[5] ZHU Cheng-yan, WU Hao, ZHU He-guo, LI Xiang-dong, TU Chun-lei, XIE Zong-han. Mechanical properties and fracture mechanism of as-cast $MnFeCoCuNi_x$ high-entropy alloys. [J]. Transactions of Nonferrous Metals Society of China, 2021, 31: 222−231.

[6] XU Jun, CAO Cheng-ming, GU Ping, PENG Liang-ming. Microstructures, tensile properties and serrated flow of $Al_xCrMnFeCoNi$ high entropy alloys [J]. Transactions of Nonferrous Metals Society of China, 2020, 30: 746−755.

[7] FU Jian-xin, CAO Cheng-ming, TONG Wei, PENG Liang-ming. Effect of thermomechanical processing on microstructure and mechanical properties of CoCrFeNiMn high entropy alloy [J]. Transactions of Nonferrous Metals Society of China, 2018, 28: 931−938.

[8] LU Yi-ping, DONG Yong, GUO Sheng, JIANG Li, KANG Hui-jun, WANG Tong-min, WEN Bin, WANG Zhi-jun, JIE Jin-chuan, CAO Zhi-qiang, RUAN Hai-hui, LI Ting-ju. A promising new class of high-temperature alloys: Eutectic high-entropy alloys [J]. Scientific Reports, 2014, 4: 6200.

[9] LU Yi-ping, GAO Xu-zhou, JIANG Li, CHEN Zong-ning, WANG Tong-min, JIE Jin-chuan, KANG Hui-jun, ZHANG Yu-bo, GUO Sheng, RUAN Hai-hui, ZHAO Yong-hao, CAO Zhi-qiang, LI Ting-ju. Directly cast bulk eutectic and near-eutectic high entropy alloys with balanced strength and ductility in a wide temperature range [J]. Acta Materialia, 2017, 124: 143−150.

[10] VAIRIS A, FROST M. On the extrusion stage of linear friction welding of Ti6Al4V [J]. Materials Science and Engineering A, 1999, 271: 477−484.

[11] SKUBISZ P, SIŃCZAK J, BEDNAREK S. Forgeability of Mg−Al−Zn magnisum alloys in hot and warm closed die forging [J]. Journal of Materials Processing Technology, 2006, 177: 210−213.

[12] ADOMAKO N K, SHIN G, PARK N, PARK K, KIM J H. Laser dissimilar welding of CoCrFeMnNi-high entropy alloy and duplex stainless steel [J]. Journal of Materials Science & Technology, 2021, 85: 95−105.

[13] DAVID S A, DEBROY T. Current issues and problems in welding science [J]. Science, 1992, 257: 497−502.

[14] GUO J F, CHEN H C, SUN C N, BI G, SUN Z, WEI J. Friction stir welding of dissimilar materials between AA6061 and AA7075 Al alloys effect of process parameters [J]. Materials & Design, 2014, 56: 185−192.

[15] ZHU Z G, SUN Y F, GOH M G, NG F L, NGUYEN Q B, FUJII H, NAI S M L, WEI J, SHEK C H. Friction stir welding of a $CoCrFeNiAl_{0.3}$ high entropy alloy [J]. Materials Letters, 2017, 205: 142−144.

[16] ZHU Z G, SUN Y F, NG F L, GOH M G, LIAW P K, FUJII H, NGUYEN Q B, XU Y, SHEK C H, NAI S M, WEI J. Friction-stir welding of a ductile high entropy alloy: Microstructural evolution and weld strength [J]. Materials Science and Engineering A, 2018, 711: 524−532.

[17] YUAN L, XIONG J T, REN J, YANG T, MA Y K, LUAN J H, LI J L. Ultrastrong and ductile transient liquid phase (TLP) bonding joints reinforced by ordered multi-precipitates [J]. Composites Part B: Engineering, 2022, 231: 109568.

[18] LI Peng, SUN Hao-tian, WANG Shuai, HAO Xiao-hu, DONG Hong-gang. Rotary friction welding of $AlCoCrFeNi_{2.1}$ eutectic high entropy alloy [J]. Journal of Alloys and Compounds, 2020, 814: 152322.

[19] SOKKALINGAM R, MUTHUPANDI V, SIVAPRASAD K, PRASHANTH K G. Dissimilar welding of $Al_{0.1}CoCrFeNi$ high-entropy alloy and AISI304 stainless steel [J]. Journal of Materials Research, 2019, 34: 2683−2694.

[20] WANG Ge, SHENG Guang-min, SUN Jian-chun, WEI Yu, GAO Xian-hui, YU Zhe, YUAN Xin-jian. Mechanical properties and microstructure evolution of CrMnFeCoNi HEA/304 SS dissimilar brazing joints [J]. Journal of Alloys and Compounds, 2020, 829: 154520.

[21] WANG Ge, SHENG Guang-min, YU Qi-li, SUN Jian-chun, LI Rui, YUAN Xin-jian, ZHANG Yun-tao. Investigation on regulating inter-granular penetration in CoCrMnFeNi high-entropy alloy and 304 stainless steel dissimilar joints [J]. Materials Science and Engineering A, 2021, 800.

[22] LI Peng, SUN Hao-tian, DONG Hong-gang, XIA Yue-qing,

WANG Shuai, HAO Xiao-hu. Microstructural evolution, bonding mechanism and mechanical properties of $AlCoCrFeNi_{2.1}$ eutectic high entropy alloy joint fabricated via diffusion bonding [J]. Materials Science and Engineering A, 2021, 814: 141211.

[23] LEI Y, HU S P, YANG T L, SONG X G, LUO Y, WANG G D. Vacuum diffusion bonding of high-entropy $Al_{0.85}CoCrFeNi$ alloy to TiAl intermetallic [J]. Journal of Materials Processing Technology, 2020, 278: 116455.

[24] LI Peng, WANG Shuai, XIA Yue-qing, HAO Xiao-hu, DONG Hong-gang. Diffusion bonding of $AlCoCrFeNi_{2.1}$ eutectic high entropy alloy to TiAl alloy [J]. Journal of Materials Science & Technology, 2020, 45: 59−69.

[25] DU Y J, XIONG J T, JIN F, LI S W, YUAN L, FENG D, SHI J M, LI J L. Microstructure evolution and mechanical properties of diffusion bonding $Al_5(TiZrHfNb)_{95}$ refractory high entropy alloy to Ti_2AlNb alloy [J]. Materials Science and Engineering A, 2021, 802: 140610.

[26] ZHANG Ya-li, JIANG Xiao-song, FANG Yong-jian, SUN Hong-liang, SONG Ting-feng, MO De-feng, LI Xue, LUO Zhi-ping. Vacuum diffusion bonding of CoCrFeNiMo MEAs and Inconel 718 using Ni interlayer [J]. Materials Letters, 2020, 279: 128509.

[27] LI Peng, SUN Hao-tian, WANG Shuai, XIA Yue-qing, DONG Hong-gang, WEN Guo-dong, ZHANG Hao. Diffusion bonding of $AlCoCrFeNi_{2.1}$ eutectic high entropy alloy to GH4169 superalloy [J]. Materials Science and Engineering A, 2020, 793: 139843.

[28] LIU Yu-lin, LUO Yong-chun, ZHAO Dan, ZHANG Guo-qing, KANG Long. Interfacial behavior and joint performance of high-entropy alloy CoCrFeMnNi and pure Cu joints obtained by vacuum diffusion welding journal of mechanical engineering [J]. Journal of Mechanical Engineering, 2017, 53: 84−91. (in Chinese)

[29] LEE J M, KANG S B, SATO T, TEZUKA H, KAMIO A. Evolution of iron aluminide in Al/Fe in situ composites fabricated by plasma synthesis method [J]. Materials Science and Engineering A, 2003, 362: 257−263.

[30] PRETORIUS R. Phase sequence of silicide formation at metal-silicon interfaces [J]. Vacuum, 1990, 41: 1038−1042.

[31] THERON C C, NDWANDWE O M, LOMBAARD J C, PRETORIUS R. First phase formation at interfaces comparison between Walser−Bené and effective heat of formation model [J]. Materials Chemistry and Physics, 1996, 46: 238−247.

[32] DABROWA J, KUCZA W, CIESLAK G, KULIK T, DANIELEWSKI M, YEH J W. Interdiffusion in the FCC-structured Al−Co−Cr−Fe−Ni high entropy alloys: Experimental studies and numerical simulations [J]. Journal of Alloys and Compounds, 2016, 674: 455−462.

[33] JUAN Wang, LI Ya-jiang, HUANG Wan-qun. Interface microstructure and diffusion kinetics in diffusion bonded Mg/Al joint [J]. Reaction Kinetics and Catalysis Letters, 2008, 95: 71−79.

[34] ZHAO Yang-yang, LI Jiu-yong, QIU Ran-feng, SHI Hong-xin. Growth characterization of intermetallic compound at the Ti/Al solid state interface [J]. Materials, 2019, 12: 472.

[35] XUE P, XIAO B L, MA Z Y. Effect of interfacial microstructure evolution on mechanical properties and fracture behavior of friction stir-welded Al−Cu joints [J]. Metallurgical and Materials Transactions A, 2015, 46: 3091−3103.

[36] LIU Yu-lin, LUO Yong-chun, SHI Yan-yan. Vacuum diffusion welding between CoCrFeMnNi high entropy and stainless steel [J]. Electric Welding Machine, 2016, 46: 122−127. (in Chinese)

[37] DAVIS J R. Properties and selection: Nonferrous alloys and special-purpose materials [M]. USA: ASM International ASM handbook, 1995.

$AlCoCrFeNi_{2.1}$ 共晶高熵合金与 304 不锈钢扩散焊接头强化新策略

李 鹏，孙浩田，李 超，吴宝生，杨 江，姜 瑀，董红刚

大连理工大学 材料科学与工程学院，大连 116024

摘 要：为探索共晶高熵合金潜在的工程应用，研究 $AlCoCrFeNi_{2.1}$ 共晶高熵合金与 304 不锈钢扩散焊接头的界面组织和力学性能。扩散区由固溶体区和 Fe_2Al_5 金属间化合物区组成。不锈钢与高熵合金、高熵合金中两相之间均存在元素扩散速率差异，近高熵合金侧形成由 FCC 相和 γ-Fe 相组成的固溶体区，提高接头的剪切强度。另外，接头剪切强度先增加后减少，在 980 ℃，60 min 和 30 MPa 工艺参数下接头最高剪切强度为 355 MPa。扩散区形成的互锁结构和局部固溶体结构协同提高接头的剪切强度。

关键词：扩散连接；$AlCoCrFeNi_{2.1}$ 共晶高熵合金；强化机理；304 不锈钢；剪切强度

(Edited by Bing YANG)